International Journal of Pharmaceutics xxx (xxxx) 124749

Contents lists available at ScienceDirect

International Journal of Pharmaceutics

journal homepage: www.elsevier.com/locate/ijpharm

Ultrasound-compatible 3D-printed Franz diffusion system for sonophoresis with microbubbles

Xin Chen [a], Davide De Grandi [b], Yonglian Zhu [a], Gareth Lutheryn [b], Majella Lane [a], Bruno Da Silva Sil Dos Santos [c], Dario Carugo [b,*]

[a] School of Pharmacy, University College London, 29-39 Brunswick Square, London WC1N 1AX, UK
[b] Nuffield Department of Orthopaedics, Rheumatology and Musculoskeletal Sciences, University of Oxford, B4495, Headington, Oxford OX3 7LD, UK
[c] London Metropolitan University, 166-220 Holloway Rd, London N7 8DB, UK

ARTICLE INFO

Keywords:
Ultrasound
Microbubbles
Sonophoresis
In-vitro diffusion system
3D printing

ABSTRACT

Sonophoresis is a topical drug delivery approach that utilises ultrasound as a physical stimulus to enhance permeation of active pharmaceutical ingredients through the skin. Only limited research has however been conducted to evaluate the potential of ultrasound-responsive drug carriers, such as gas microbubbles, in sonophoresis. Franz diffusion cells have been extensively used for measuring drug permeation *in vitro*; however, traditional systems lack compatibility with ultrasound and only limited characterisation of their acoustical behaviour has been carried out in previous research. To overcome this limitation, we designed and manufactured a novel Franz cell donor compartment coupled with a conventional glass receptor, and performed a functional characterisation of the assembly for application in sonophoresis with ultrasound-responsive agents (specifically imiquimod-loaded gas microbubbles). The donor was fabricated using a photoreactive resin *via* 3D printing and was designed to enable integration with a therapeutically relevant ultrasound source. The assembly was capable of effectively retaining liquids during prolonged incubation and the absorption of imiquimod onto the 3D-printed material was comparable to the one of glass. Moreover, a predictable ultrasound field could be generated at a target surface without any significant spatial distortion. Finally, we demonstrated applicability of the developed assembly in sonophoresis experiments with StratM®, wherein ultrasound stimulation in the presence of microbubbles resulted in significantly enhanced drug permeation through and partitioning within the membrane (2.96 ± 0.25 μg and 3.84 ± 0.39 μg) compared to passive diffusion alone (1.74 ± 0.29 μg and 2.29 ± 0.32 μg), over 24 h.

1. Introduction

Sonophoresis is a method that uses ultrasound (US) to physically enhance topical drug delivery. It has shown potential to increase skin permeability of different classes of substances, including lipophilic, hydrophilic, and high molecular weight molecules (Dahlan et al., 2009; Hakozaki et al., 2006; Meidan et al., 1999; Mitragotri and Kost, 2001; Park et al., 2007). Ultrasound comprises pressure waves that are typically generated by a piezoelectric transducer – a device that converts an electrical signal into a mechanical pressure wave of frequency > 20 kHz. In topical applications, the transducer is placed on the skin's surface using a coupling medium (Petrilli and Lopez, 2018). The primary mechanism governing sonophoresis is hypothesised to be cavitation, which refers to the formation and/or volumetric oscillation (i.e., alternating expansion and contraction) of gas bubbles upon exposure to ultrasound waves (Liu et al., 2023). When bubbles undergo cavitation in the vicinity of a surface (such as the skin), their oscillation is asymmetrical and – upon bubble collapse – the generated high-speed microjets can deliver mechanical energy onto localised regions of tissue to increase its permeability (Isselin et al., 1998).

Sonophoresis most commonly relies on the formation of endogenous air nuclei induced by the ultrasound pressure wave; these can however form at randomly distributed locations within intercellular and intracellular spaces and may also generate within the coupling medium. These gas bodies appear to respond most effectively to low-frequency ultrasound (20–100 kHz), with ultrasound penetration depth and cavitation intensity being inversely correlated with the ultrasound frequency (Gaertner, 1954). The application of low-frequency ultrasound,

* Corresponding author at: Nuffield Department of Orthopaedics, Rheumatology and Musculoskeletal Sciences, University of Oxford, B4495, Headington, Oxford OX3 7LD, UK.
E-mail address: dario.carugo@ndorms.ox.ac.uk (D. Carugo).

https://doi.org/10.1016/j.ijpharm.2024.124749
Received 27 June 2024; Received in revised form 21 September 2024; Accepted 22 September 2024
0378-5173/

however, carries the risk of skin and organ damage (Ahmadi et al., 2012), and the lack of control over the size and concentration of endogenous cavitation nuclei can impact on treatment controllability and repeatability (Park et al., 2022). Conversely, high-frequency ultrasound (>100 kHz) has a long-term safety record in clinical settings and may present a more clinically viable alternative (Polat et al., 2011). However, cavitation of relatively large endogenous gaseous nuclei is inefficient at higher ultrasound frequencies, hindering the ability of this method to permeabilise the stratum corneum and increase drug penetration depth (Tyle and Agrawala, 1989). Gas microbubbles (MBs) with a mean diameter of approximately 1–3 μm can also be produced in the laboratory and employed as exogenous cavitation nuclei. They are often stabilised by a layer of phospholipids and, given their smaller size, they can be induced to efficiently cavitate when exposed to high-frequency ultrasound (typically in the range 0.5–2 MHz), resulting in enhanced transdermal delivery of bioactive molecules (Park et al., 2022, 2012). Therefore, the combined application of high-frequency US with exogenous microbubbles of defined characteristics (such as size and concentration) could provide a safer and more controllable alternative to low-frequency US in sonophoresis.

Franz diffusion cells are the most commonly used apparatus for *in-vitro* drug permeation studies. These cells comprise three main parts, namely (from top to bottom): (i) the donor, (ii) a skin tissue or model, and (iii) the receptor (Simon et al., 2016). They are commonly manufactured from annealed borosilicate glass and are designed for passive drug diffusion experiments. However, glass has a relatively high acoustic impedance (14.08 MRayls, at an ultrasound frequency of 1.1 MHz), which is defined as the resistance that a material offers to the propagation of an US wave through it. This in turn results in an ultrasound reflection coefficient for a water–glass interface of 0.654, indicating that approximately two-thirds (65.4 %) of an ultrasound wave travelling through water undergoes reflection when it encounters a glass surface (Beamish et al., 2022). The application of US within a conventional diffusion Franz cell is therefore likely to result in the generation of ultrasonic standing waves that negatively impact on the spatial uniformity of the acoustic pressure field over the treated area. The use of these cells in sonophoresis-related research may thus present several drawbacks, as highlighted in Table 1. In addition to the formation of standing waves, there are limitations associated with the manual positioning of the transducer (which can introduce variability in US exposure conditions and cavitation activity across experimental repeats) and difficulties in measuring the acoustic field within systems with a small footprint (preventing a quantitative characterisation of the stimulation conditions). In recent years, uncertainties surrounding sonophoresis have gained increasing attention (Robertson and Becker, 2018), and several studies have focused on modifications of the experimental setup to mitigate limitations associated with conventional Franz cells. However, these modified systems still suffer from limitations (see Table 1) such as large priming volumes or limited precision in the positioning of the US source, hindering their usability in conjunction with US-responsive agents.

Additive manufacturing (commonly known as 3D printing) based on high-resolution stereolithography (SLA), is an emerging technology that has been used for manufacturing customised parts in experimental research (Mohmmed et al., 2017). The ease of model design, user-friendly operation, combined with a diverse range of usable printing materials, render 3D printers an indispensable apparatus in numerous scientific applications (Mohmmed et al., 2017; Norman et al., 2017). Moreover, photoreactive resins used in SLA printing have greater ultrasound compatibility than glass. These polymeric resins have acoustic impedance of 2–3 MRayls, resulting in only 0.58 % to 2.4 % of the incident US wave being reflected at a water-resin interface (Trogé et al., 2010). Limiting the extent of US reflections can mitigate the generation of ultrasonic standing wave fields, which would cause spatial inhomogeneities in the acoustic pressure field (Saito, 2015). Overall, if applied to a Franz cell apparatus, this can result in improved uniformity of the acoustic pressure field acting over the target skin surface (Robertson and Becker, 2015). A limitation associated with SLA for the manufacturing of Franz cells is the potential drug retention resulting from the use of acrylate-based resins, as reported in previous studies (Bendicho-Lavilla et al., 2024; Sil et al., 2020, 2018). Acrylate-based resins can be classified into hydrophobic (such as methyl methacrylate) and hydrophilic (such as glycol methacrylate) (Stirling and Woods, 2019). Some drugs have been reported to undergo chemical interactions with the methacrylate groups of the resin (Sil et al., 2018). During printing, the acrylate monomers undergo photopolymerization by free radical chain reaction and subsequent curing. The presence of acrylate-based resin residues on partially cured surfaces, can result in physical and chemical interactions with drugs as well as increased water absorption (Salonitis, 2014; Tiboni et al., 2021). On the other hand, epoxy-based resins exhibit hydrophilic properties due to their epoxy group (Palanisamy et al., 2017; Sindhu et al., 2021). They undergo cationic-initiated polymerization in the presence of cationic photoinitiators, and the polymerization reaction continues even after the cessation of irradiation. Consequently, these resins tend to achieve complete polymerization with minimal residues remaining on the surface of a model (Salonitis, 2014). When epoxy-based resins were applied as a coating to 3D-printed models in previous research, they were able to effectively prevent drug retention (Bendicho-Lavilla et al., 2024).

In order to overcome some of the limitations of devices employed in previous research assessing microbubble-mediated sonophoresis, in this study we developed an ultrasound-integrated Franz diffusion cell for application with US-responsive particulate systems. It comprises a conventional glass receptor, a metal clamp, and a novel donor design man-

Table 1
A summary of previous studies using Franz diffusion cells for *in-vitro* research on drug delivery by sonophoresis.

Franz cell type		Sample type (in donor)	Advantages	Disadvantages	Reference
Donor	Receptor				
Original	Original	Water	N/A	Potentially limited repeatability of the acoustic field	(Liao et al., 2021; Souza et al., 2013; Subongkot, 2020; Wolloch and Kost, 2010; Zhang et al., 2017)
Original	No	Water	No US reflection from the receptor walls	Did not measure the acoustic field properties	(Herwadkar et al., 2012)
No	Original	Water (in large water tank)	Predictable acoustic pressure field	Not suitable for US-responsive drug carriers	(Schoellhammer et al., 2012; Yamashita et al., 1997)
Original	Original	Fluorescent drug carriers	US positioning system	Potentially limited repeatability of the acoustic field	(Park et al., 2019, 2012)
No	Petri dish	Drug-loaded gel	Reduced US reflection in the donor	Manual US source positioning	(Jung et al., 2016)
Customised glass (larger)	Original	Liquid-core nuclei in PBS	Reduced US reflection in the donor	Increased sample size and uneven US treatment	(Park et al., 2022)
Customised glass (trapezoid)	Original	Drug-loaded microbubbles in PBS	Compatible with an US transducer	Potentially limited repeatability of the acoustic field	(Wang et al., 2016; Yu et al., 2023)

ufactured through 3D printing. Moreover, the device was characterised quantitatively for: its ability to retain liquid samples, drug adsorption onto the 3D-printed material, acoustic performance, as well as suitability for US and microbubble-mediated permeation research.

2. Materials and methods

2.1. Materials

Resins suitable for printing transparent parts by stereolithography were purchased from Formlabs (Formlabs® Clear; Formlabs, Massachusetts, USA) and 3D systems (Accura® ClearVue; 3D systems, Los Angeles County, California, USA). 1,2-distearoyl-*sn*-glycero-3-phosphocholine (DSPC; $M_w \approx 790$ Da) was purchased from Avanti Polar Lipids Inc. (Alabaster, Alabama, United States). Imiquimod (IMQ; 99.9 %) was purchased from Thermo Fisher Scientific Inc. (Loughborough, UK). Polyoxyethylene 40 stearate (PEG40S; $M_w \approx 2046$ Da), polyoxyethylene (20) cetyl ether (Brij® 58), StratM® membrane, phosphate buffer saline (PBS) tablets, sodium acetate (HPLC grade), acetate acid (≥99.9 % purity), triethylamine (99 % purity), acetonitrile (≥99.9 % purity), high performance liquid chromatography (HPLC) grade water, methanol (≥99.9 % purity), and chloroform (≥99 % purity) were purchased from Sigma-Aldrich Ltd. (Gillingham, Dorset, UK).

2.2. Design rationale for the US-integrated Franz diffusion cell

Optical transparency is an essential feature of Franz diffusion cells, as it enables visual inspection of the apparatus to ensure a hermetic assembly and the complete elimination of any trapped air pockets. This latter requirement is particularly important for applications involving ultrasound, as the presence of large air pockets within the ultrasound path would prevent efficient US propagation to a target surface or tissue. To meet this design requirement, clear resins were selected as the constitutive material for the donor compartment (whilst a standard glass receptor was used, as discussed below). The delivery of ultrasound into the Franz cell requires maintaining a water-filled pathway between the ultrasound source (i.e., the transducer) and the skin model, to minimise US attenuation or distortions of the acoustic field caused by undesired reflections. Transducers that are capable of delivering therapeutically relevant acoustic pressures are relatively large in size (i.e., often with a diameter of several centimetres) when compared to the size of a Franz cell; therefore, direct interfacing between the two systems is not practical. For this reason, the transducer was coupled with a transparent cone filled with water. Notably, the smaller terminal section of the cone could be coupled more easily with the donor compartment. For studies involving the use of US-responsive particles, the donor design should also enable injection of the particle suspension at desired timepoints. To meet these additional design requirements, a new donor design was conceptualised, characterised by three main changes compared to a conventional Franz diffusion cell: (i) a V-shaped feature to enable efficient and stable integration with the water-filled transmission cone of the transducer; (ii) a smaller height to reduce the separation distance between microbubbles and the treated surface; and (iii) a lateral port through the donor's wall for injection of a microbubble suspension.

Since only trace amounts of a drug may permeate through a skin sample or model, it was decided to maintain the conventional glass-based configuration for the receptor compartment, to minimise potential drug adsorption onto a porous 3D-printed resin.

2.3. Design of the US-integrated Franz cell

The dimensions of a conventional borosilicate glass Franz cell routinely employed at the UCL School of Pharmacy were measured using a calliper with accuracy of 0.03 mm (Accu Ltd., Huddersfield, UK), and were used as a reference for developing the modified donor design. TinkerCAD™ (Autodesk®, California, USA) was utilised for technical drawing purposes throughout this study. As shown in Fig. 1A, the Franz cell donor was designed to accommodate a microbubble suspension volume of 1 mL. The V-shaped top feature of the cell had a height of 6.6 mm and was designed for coupling with the terminal end of the transducer's cone (as shown in Fig. 1B). It had an inner diameter (I.D.) that increased from 9.4 mm (lower end) to 27 mm (higher end), with a wall thickness correspondingly increasing from 1 mm to 2 mm for enhanced mechanical strength. The donor chamber had an I.D. of 11 mm, consistent with the size of conventional glass-based diffusion cells. The height of the chamber was designed to be slightly shorter than in the conventional Franz cell, in order to accommodate precisely 1 mL of sample. The bottom section of the donor had an outer diameter (O.D.) of 30 mm, to enable coupling with a commercial glass receptor. Compared with a conventional diffusion cell, the thickness of this section was increased from 2 mm to 3 mm for improved mechanical strength. A side-port (O.D. = 4 mm; thickness = 1 mm) was designed to enable injection of a microbubble suspension and removal of any exogenous air pockets present in the chamber before ultrasound treatment.

2.4. Fabrication of the Franz cell donor compartment

The Franz cell donor was fabricated using clear polymeric resin (Formlabs® Clear and Accura® ClearVue) *via* SLA 3D printing; the physico-chemical properties of the resins are listed in Table 2. The model designed in TinkerCAD™ was initially transferred into Preform (3D software; version 3.24.2). The design was rotated to a specific angle (45°) to establish the mechanical supports required during printing (point size: 0.50 mm, point density: 1). To ensure a flat bottom surface of the printout, any support touching the top surface of the design was removed. Following the printing process, the parts were rinsed with isopropanol for 10 min to eliminate any uncured resin. Subsequently, the models underwent post-curing under UV light at a wavelength of 405 nm for 30 min. Once polymerised, the support structures were carefully removed using scissors and a polishing process was applied to smoothen any potential imperfection.

2.5. Sealing performance of the developed Franz cell

Tests were carried out to ensure that the newly developed donor-receptor assembly could effectively retain liquid samples, without any leakage taking place. This is a necessary prerequisite for effective usage of the system in drug permeation studies. The following experimental steps were carried out for this purpose: (i) a polydimethylsiloxane (PDMS) membrane was securely clamped using a Franz cell clamp, with a small amount of silicone grease (SG M494 Silicone Grease) applied between the donor and receptor compartments; (ii) PBS with 1 % Brij 58® was injected into the receptor chamber through its side-port using a 5 mL syringe (IV syringe Luer slip), ensuring removal of any air pocket; (iii) 1 mL of PBS was injected into the donor compartment, which was then sealed with a custom-built PDMS lid; (iv) a small magnetic stirring bar was added into the receptor chamber through the side-port to maintain continuous stirring during the test (mimicking conditions of a drug permeation study); (v) the device was weighed using a 0.1 mg resolution balance (Sigma W3200; accuracy of 0.1 μL of water); (vi) the device was left in a 32 °C thermostatically controlled water bath (Grant London, UK) for 24 h, with the fluid in the receptor being stirred at 200 rpm; the temperature level corresponded to the recommended skin surface temperature for *in vitro* percutaneous penetration studies (Skelly et al., 1987); and finally (vii) the device was removed from the water bath, dried using optical tissue wipes, and subsequently re-weighed. The water loss from the device was calculated as follows:

$$Waterloss(g) = |m_a - m_b| \quad (1)$$

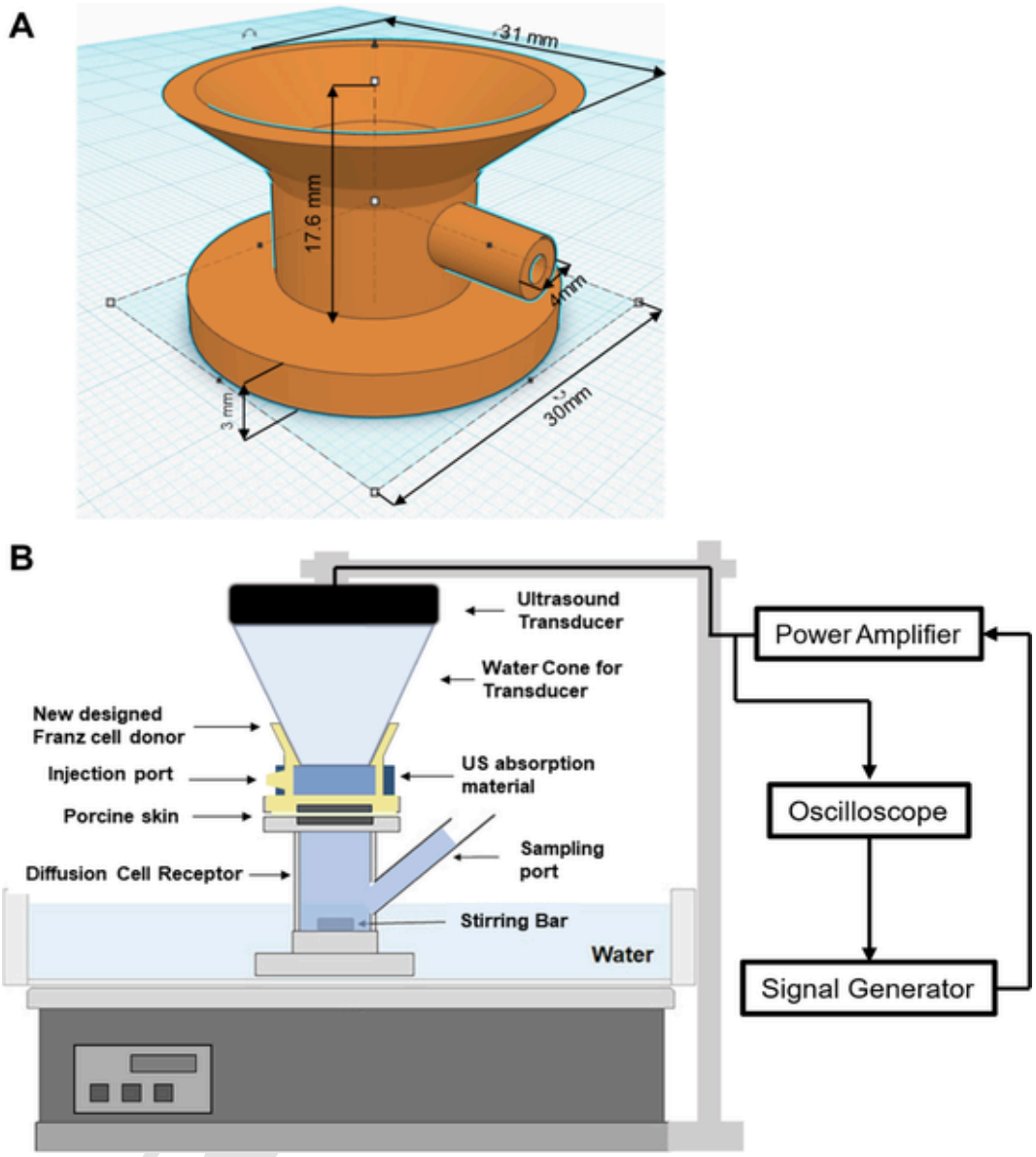

Fig. 1. (A) Design of the 3D-printed Franz cell donor (volume capacity = 1 mL) generated in TinkerCAD™. The total height is 17.6 mm and the O.D. of the bottom section is 30 mm. The V-shaped feature has an I.D. of 9.4 mm (bottom end) and 27 mm (top end). The donor chamber has an I.D. of 14 mm. (B) Schematic of the experimental set-up employed for operating the developed US-integrated Franz cell system. The ultrasound transducer (in black) is coupled to the V-shaped feature of the donor (in yellow), *via* a water-filled transmission cone (in blue). The donor, externally covered with US absorbing material, was securely clamped to the receptor, with a skin model sandwiched in between. The sample within the receptor was heated and stirred using a water bath. A power amplifier, oscilloscope, and signal generator were employed to drive and monitor the ultrasound transducer for delivering the desired ultrasound field. (For interpretation of the references to colour in this figure legend, the reader is referred to the web version of this article.)

where m_a and m_b are the mass of the device at the beginning and end of the test, respectively. Three independent experimental repeats were carried out to assess the sealing performance of the system.

2.6. Evaluating absorption of imiquimod onto 3D-printed Franz cell donors

Imiquimod was employed as a model drug in this study. Given its high hydrophobicity, it can be loaded directly within the phospholipid shell of gas microbubbles (Kotopoulis et al., 2022). Conversely, drugs that present low encapsulation efficiency within lipid-shelled microbubbles (such as hydrophilic drugs or large molecules) could be loaded onto microbubbles either by (i) direct binding (for example, through electrostatic interaction) or by (ii) loading within nanoparticulate systems (such as liposomes) that are subsequently bound to the microbubble's outer surface (i.e., through a biotin-avidin or covalent linkage). These processes would however increase formulation costs, length, and/or complexity (Lentacker et al., 2009). IMQ is therefore a suitable model compound for evaluating the feasibility of use of the developed Franz cell apparatus in studies of microbubble-mediated sonophoresis. A series of experiments were initially carried out to assess whether IMQ would be absorbed onto the 3D-printed resin of the donor, which may negatively impact on the accuracy of drug permeation readouts.

The donor and receptor were securely fastened together using a metallic clamp. A glass layer was employed as a barrier between the compartments in these tests, to prevent drug diffusion from the donor

Table 2
The physico-chemical properties of the Formlabs® Clear and Accura® ClearVue resins employed in the present study to manufacture Franz cell donors by SLA printing.

	Formlabs® Clear	Accura® ClearVue
Main polymer	7,7,9 (or 7,9,9)-trimethyl-4,13-dioxo-3,14-dioxa-5,12-diazahexadecane-1,16-diyl bismethacrylate	4,4′-Isopropylidenedicyclohexanol; oligomeric reaction products with 1-chloro-2,3 epoxypropane
Molecular weight of main polymer (Da)	470.56	332.91
Photoinitiator	Radical photoinitiator	Cationic photoinitiator
Appearance after photo-polymerization	Transparent solid	Transparent solid
Solid density	<1.16 g/cm^3	1.17 g/cm^3
Resin type	Acrylate-based	Epoxy-based
Hydrophobicity	Hydrophobic (Sil et al., 2018; Stirling and Woods, 2019)	Hydrophilic (Salonitis, 2014; Sindhu et al., 2021)
Water absorption	0.54 %	0.3 %

into the receptor. IMQ was dissolved in 100 mM sodium acetate buffer (pH 4) to a concentration of 450 μg/mL. After addition of 1 mL of IMQ solution to the donor, the device was weighed and sealed with a PDMS lid. Subsequently, the system was placed in a water bath maintained at 32 ˚C for 24 h. The amount of liquid sample evaporated was determined by measuring the weight difference of the device before and after incubation. Following the incubation period, aliquots of 200 μL were taken from the donor and appropriately diluted. HPLC analysis was used to quantify the IMQ concentration before and after incubation, and the IMQ recovery was calculated as follows:

$$Imiquimodrecovery(\%) = [1 - (C_a \times V_a)/(C_b \times V_b)] \times 100 \quad (2)$$

where C_b and C_a are the concentration of IMQ before and after incubation, m_b and m_a are the volume of the IMQ sample before and after incubation. The HPLC method used has been reported and validated in previous research (Paula et al., 2008).

2.7. Acoustic characterisation of the developed Franz diffusion cell

Determining the acoustic field properties of an experimental system developed for studying US-mediated drug delivery is an essential prerequisite to enable experimental reproducibility across laboratories as well as optimisation of the US exposure conditions for achieving desired therapeutic outcomes.

A schematic of the experimental setup that was used in these tests is shown in Fig. 2. The 3D-printed donor was assembled together with the glass receptor and a PDMS membrane sandwiched between the compartments. The device was fixed to a custom-designed holder and submerged in a water tank, for optimal acoustic coupling and control over the liquid temperature conditions (maintained at 25 ˚C). A computer-controlled positioning stage, securely installed on an external frame above the tank, was utilised to insert a 0.2 mm diameter needle hydrophone (NH-0200, Precision Acoustics, Dorchester, UK) into the donor. A 5 × 8 mm^2 rectangular opening was created on the side wall of the donor for hydrophone's insertion. The hydrophone was manipulated precisely (accuracy of 0.1 mm) to scan a 4 × 4 mm^2 area centred to the target surface and vertically across a 4 × 6 mm^2 region in the middle of the donor chamber. A power amplifier was driven by a programmable signal generator to input 20 ± 0.5 Volts peak-to-peak into a 1.1 MHz ultrasonic transducer (Sonic Concepts, model H-151 E-35). A digital storage oscilloscope (44 Xi Waverunner, Teledyne LeCroy, Chestnut Ridge, NY, USA) was employed to record both the received signal from the hydrophone and the input signal to the transducer. A custom-developed script in MATLAB R2021b (The MathWorks, Natick, MA, USA) was used to determine the received acoustic pressure at each point within the scanned region of interest.

2.8. Production of imiquimod-loaded microbubbles

IMQ-loaded microbubbles were produced following a well-established method comprising lipid film hydration followed by tip sonication (Carugo et al., 2017). Briefly, 10 mg of IMQ were dissolved in 200 mL of chloroform to prepare an imiquimod stock solution at a concentration of 500 μg/mL. 621 μL DSPC and 447 μL PEG-40S (in chloroform) were pipetted into a 15 mL vial at a molar ratio of 9:1, followed by the addition of an appropriate quantity of imiquimod solution to achieve a drug-to-lipid ratio of 3:4. The mixture was left on a hotplate

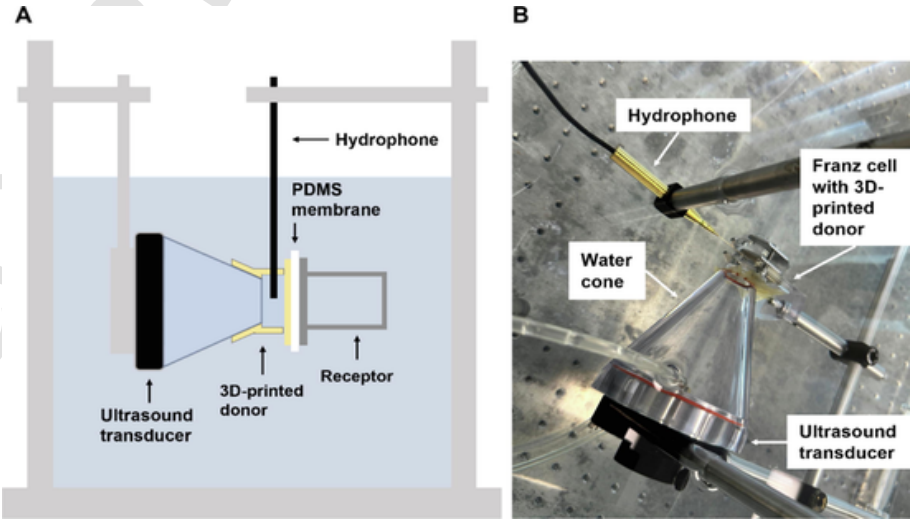

Fig. 2. Schematic illustration (left) and top-view photograph (right) of the experimental setup used to assess the ultrasound field properties within the developed Franz cell assembly. The 3D-printed donor was assembled with the glass receptor and the PDMS membrane, and then submerged in a water tank (oriented horizontally). The transducer was precisely combined with the V-shaped structure of the 3D-printed donor. The hydrophone was inserted into the donor through the lateral opening.

at 40 °C overnight to remove all of the organic solvent and form a uniform dry film at the bottom of the vial. The lipid film was then hydrated using 5 mL of PBS at 80 °C (i.e., above the phase-transition temperature of the lipids), upon stirring at 700 rpm for 60 min. The sample was then homogenously dispersed for 150 sec using a tip sonicator (Fisherbrand™ Model 120 Sonic Dismembrator, 20 kHz, 120 W, Fisher Scientific Inc, Loughborough, UK) at 40 % power, with the tip fully submerged in the liquid. Subsequently, air-filled microbubbles were generated by raising the sonicator tip to the air–water interface, and further sonicating at 70 % power for 30 sec. After sonication, the microbubble suspension was kept in an ice box for at least 5 min. The suspension was then centrifuged (200 RCF, 5 min, 4 °C) to remove any excess imiquimod and MBs were resuspended in 5 mL of PBS.

2.9. Optimization of the ultrasound treatment time

It was necessary to identify an appropriate duration for the US treatment, to ensure that a sufficient number of microbubbles would undergo cavitation and mechanical disruption, without resulting in an excessive temperature rise that may cause hyperthermia-induced damage to the skin. The experimental setup used in these tests is shown in Fig. 1B. A power amplifier (model 1040L, Electronics and Innovation, LTD, New York, USA) driven by a programmable signal generator (Aim-TTi TG 2000, Aim and Thurlby Thandar Instruments, Cambridgeshire, UK) was used to input the appropriate signal frequency (1.1 MHz) and voltage (20 Volts peak to peak) to the transducer which provided an acoustic pressure of ~ 1 MPa at the tip of the transducer cone. Notably, an ultrasound frequency of approximately 1 MHz is often employed in studies combining US with lipid-shelled microbubbles for therapeutic applications (Carugo et al., 2017). A digital oscilloscope (Tiepie Handyscope HS5, SNEEK, The Netherlands) was connected to the signal generator to monitor the sine wave produced by the power amplifier. A pulsed ultrasound field was generated, with a duty cycle of 50 %, a pulse repetition frequency (PRF) of 200 Hz, and a maximum peak-to-peak pressure at the membrane of 1.2 MPa. The Franz cell was assembled with the 3D-printed donor, a PDMS membrane, and the glass receptor. The IMQ-loaded microbubbles were diluted to a concentration of 2.25×10^8 MB/mL and injected into the 3D-printed donor through its side-port, while PBS was used to prime the receptor. Ultrasound was applied to the sample at exposure times of 15, 30, 60, 90 and 120 sec. Before and immediately after ultrasound exposure, 10 μL of the MB suspension were collected and pipetted into a Neubauer haemocytometer counting chamber (Sigma-Aldrich Ltd., Gillingham, Dorset, UK) for image capture at 40 × magnification using a Leica DM500 microscope coupled with a CCD camera (Leica Microsystems GmbH, Germany). These images were captured from 10 randomly selected positions and processed using Image J to calculate the MB concentration. The percentage destruction rate of MBs by ultrasound was calculated as follows:

$$Destructionrate\,(\%) = [(C_b - C_a)/C_b] \times 100 \quad (3)$$

where C_b is the MB concentration before ultrasound exposure and C_a is the MB concentration after ultrasound exposure.

To assess potential changes in the fluid temperature due to US application, a 32 °C PBS solution was utilised as a substitute for the microbubble suspension and subjected to ultrasound treatment with identical exposure times. The temperature was recorded in proximity to a membrane used as a skin model (i.e., StratM® membrane) using a temperature probe (IKA® ETS-D5 temperature controller), before and immediately after each treatment. The difference between these two values was then calculated as a measure of ultrasound-induced temperature increase.

2.10. In-vitro permeation studies of IMQ-loaded microbubbles

Tests were carried out to assess whether the developed Franz cell apparatus could be employed to evaluate permeation enhancement by US-responsive microbubbles. Permeation studies in the absence of US exposure were conducted using both 3D-printed and glass donors, for comparison. IMQ-loaded microbubbles were employed as a model US-responsive formulation and StratM® as an artificial skin model. The receptor was filled with PBS containing 1 % Brij 58 (pH 7.3 ± 0.1) in all experiments. After equilibrating the StratM® membrane to a temperature of 32 °C, the microbubble suspension (1 mL) was added to the donor. For the ultrasound treatment group, the US parameters were: 1.1 MHz frequency, 200 Hz PRF, 50 % duty cycle, 1.2 MPa acoustic pressure at the membrane, and 30 sec of total treatment time. A PDMS lid was employed to seal the donor post-stimulation and prevent sample evaporation. 200 μL of sample were removed from the receptor compartment at different time intervals (0, 0.25, 0.5, 0.75, 1, 1.5, 2, 3, 4, 5, 6, 7, 8, 9, 10, 11, 12, and 24 h), and replaced with fresh PBS (at 32 °C) containing 1 % Brij 58. At the end of the study, the StratM® membrane was cleaned and incubated with methanol, and the sample that remained in the donor was recovered. These samples were then diluted appropriately for measuring concentrations by HPLC analysis. The cumulative amount of permeated IMQ was quantified over time, and values were normalized to the permeated area of the membrane.

3. Results and discussion

3.1. Evaluating the sealing performance and IMQ absorption of 3D-printed Franz cell donors

Experiments were first conducted to assess whether assembling a custom-developed 3D-printed donor with a commercial glass receptor would maintain an effective seal. Efficient sealing performance during prolonged incubation is crucial as fluid leakages may result in the generation of air pockets that may interfere with US propagation, as well as cause changes in drug concentration that would compromise the accuracy of drug permeation measurements. The quantified sample losses, expressed in terms of mass of water (in grams), are shown in Fig. 3A for donors made of resin (either Formlabs® Clear or Accura® ClearVue) and borosilicate glass (commercial donor design). It should be noted that the balance used has an accuracy of 0.0001 g (corresponding to ~ 0.1 μL of water). The different donor types had comparable performance with minimal water loss, at both 6 and 12 h. After 24 h incubation, the donor manufactured using Formlabs® Clear showed higher levels of sample loss compared with the ones made with Accura® ClearVue or glass. The water loss was however equal to only ~ 4 μL for the Formlabs® Clear donor, corresponding to ~ 0.4 % of the total sample volume. Considering that both resin-based donors employ an identical design, the slight difference in performance is likely attributable to inherent material characteristics. According to technical data reports, the water absorption of Formlabs® Clear and Accura® ClearVue is 0.54 % and 0.3 %, respectively, under identical test conditions (ASTM D570-98 2018) (3D Systems, 2014; Formlabs, 2016). Greater water absorption of Formlabs® Clear may be because of the corresponding greater porosity for this resin, resulting in increased moisture evaporation through the material (Pero et al., 2011).

The use of glass as a constitutive material of Franz cell donors is common in drug permeation studies, as it exhibits minimal interaction with permeants (Sil et al., 2018). With the advent of 3D printing in this area of research, previous studies have evaluated the potential interaction between photocurable resins and different classes of molecules. Therefore, the compatibility of resins with IMQ was evaluated in the present study, prior to conducting permeation studies (Sil et al., 2018). The percentage of IMQ recovered from the Accura® ClearVue resin donor upon incubation at 32 °C for 24 h was of approximately

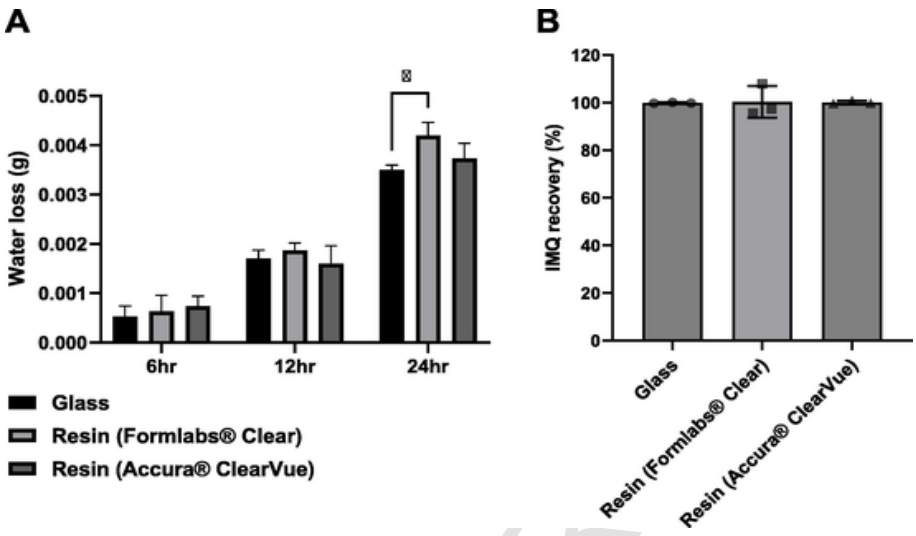

Fig. 3. (A) Water loss from the Franz cell assembly after 6, 12 and 24 h (upon stirring). (B) The % recovery of imiquimod (IMQ) from the Franz cell donor after 24 h. In both (A) and (B) the Franz cells consisted of a conventional borosilicate glass receptor, a PDMS membrane, and a donor fabricated using either glass, Formlabs® Clear resin, or Accura® ClearVue resin (n = 3 independent experiments, mean ± SD, two-way ANOVA with paired *t*-test, * means $p < 0.05$).

100.03 ± 0.58 %, and there was no significant difference between the two resin types and glass (Fig. 3B, ANOVA, $p > 0.05$). These results demonstrate that a resin-based Franz cell donor exhibits excellent compatibility with a hydrophobic drug such as IMQ. However, the performance was more variable for 3D-printed resin donors compared with the glass donor (as manifest in the greater standard deviation of IMQ % recovery in Fig. 3B), and particularly for donors printed using Formlabs® Clear. This observation could be attributed to the greater porosity of Formlabs® Clear, resulting in increased absorption of a low molecular weight permeant such as IMQ (molecular weight of 240.304 Da) (Zaleski et al., 2009). Moreover, the Formlabs® Clear is an acrylate-based resin with a relatively hydrophobic character, and the methacrylate groups of the resin may further enhance its interaction with hydrophobic compounds (Sil et al., 2018). Conversely, Accura® ClearVue has a hydrophilic character due to the presence of polar epoxy groups and demonstrated a weaker interaction with IMQ. This latter resin was thus chosen as the most appropriate material for subsequent permeation studies (Palanisamy et al., 2017; Salonitis, 2014; Sindhu et al., 2021). There are several factors contributing to drug retention on the material of 3D-printed models, including surface porosity, presence of residual uncured resin, and drug interactions with functional groups of the resin. (Salonitis, 2014; Sil et al., 2018; Zaleski et al., 2009). Whilst the present study provides a proof-of-concept evaluation of a novel technology platform for investigating microbubble-mediated sonophoresis, it is essential that the compatibility between selected drugs and 3D-printed materials is assessed in any future study utilising this and/or comparable systems. As discussed earlier, glass was instead selected as the constitutive material for the receptor compartment.

3.2. Properties of the ultrasound field within the developed Franz cell assembly

Experiments were performed to characterise the ultrasound field generated within the developed Franz cell assembly, and to assess whether potential distortions to the field may be caused by the interaction between the incident ultrasound wave and the walls of the device. The acoustic pressure inside the donor chamber of the set-up was measured by positioning the hydrophone in orthogonal orientation. The sensitivity of the hydrophone in both orthogonal and axial orientation were measured, yielding values of 27.3 mV/MPa and 40.7 mV/MPa, respectively. Positioning the hydrophone in orthogonal orientation therefore results in a 32.92 % decrease in sensitivity compared to the axial orientation, and this was taken into account when processing the recorded acoustic pressure data. Fig. 4A shows the spatial contours of peak-to-peak acoustic pressure (at 1.1 MHz ultrasound stimulation frequency) over a 4 × 4 mm^2 area, precisely centred with the surface of the skin model (i.e., a PDMS membrane in this case). The hydrophone was positioned above and in close proximity to the membrane to prevent any damage upon direct contact. Notably, the measured acoustic pressure field was almost undistorted, with greater pressure in the central region that gradually reduced towards more peripheral regions. There was only a slight asymmetry in the field that likely resulted from the creation of a lateral opening in the donor chamber for insertion of the hydrophone. These observations indicate the absence of any significant US reflection taking place at the inner walls of the 3D-printed donor compartment, which is likely due to the acoustic impedance of the resin being closer to that of water (when compared to a glass donor). Importantly, the generated acoustic pressure magnitude (1.2 MPa peak-to-peak) is well within the range that is commonly employed in therapeutic applications of ultrasound (Sen et al., 2015). The acoustic pressure field was also characterised at different vertical positions away from the transmission cone (progressively moving towards the PDMS membrane), as shown in the peak-to-peak acoustic pressure contours of Fig. 4B. Results reveal an expected reduction in the pressure magnitude from the terminal end of the cone towards the membrane, as well as the presence of alternating pressure maxima (referred to as 'pressure antinodes') and pressure minima (referred to as 'pressure nodes'). The latter observation is indicative of the generation of a standing wave field, resulting from the interaction between the forward incident US wave generated by the transducer and a backward wave. This hypothesis is corroborated by the results reported in Fig. 4C, showing the signal recorded by the hydrophone over time at a fixed position above the membrane. It took 69.5 μs for the US wave to travel from the transducer to the hydrophone, indicating that the hydrophone was positioned only 1.2 mm above the membrane (calculated assuming a speed of sound in water of 1498 m/s). A second wave of lower amplitude was recorded after 26 μs from the initial incident wave. It is hypothesised that this second wave originated from part of the incident wave being reflected backwards at the interface between the liquid and the bottom glass surface of the receptor (i.e., the water–glass interface has an ultrasound reflection coefficient of 65.4 %). It was estimated that the distance between the hydrophone and the reflecting surface

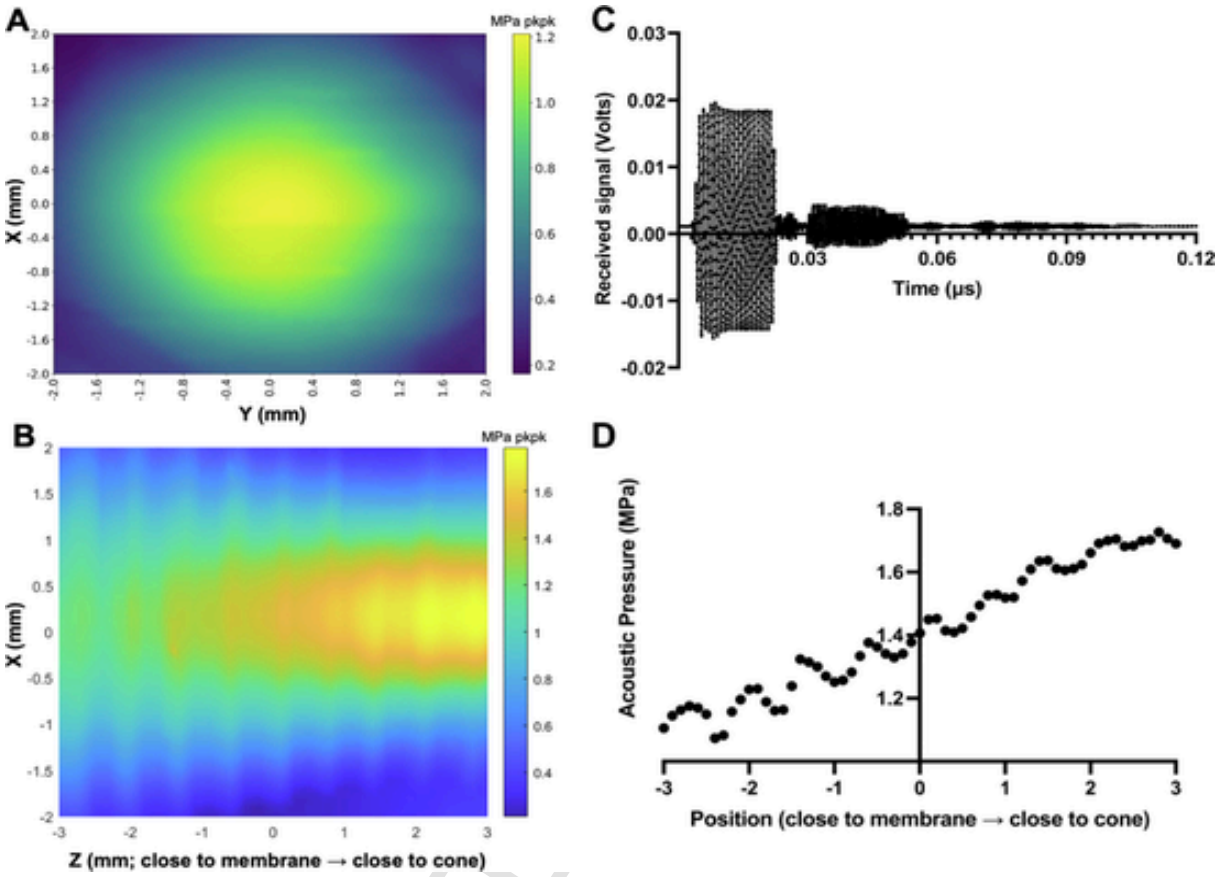

Fig. 4. Acoustic characterisation of the developed Franz cell assembly. (A) Contours of peak-to-peak acoustic pressure (in MPa) over a 4 × 4 mm^2 area centred with the skin model (and positioned just above the membrane). (B) Contours of peak-to-peak acoustic pressure (in MPa) over a 4 × 6 mm^2 vertical cross-sectional area positioned centrally within the donor. (C) Time evolution of the signal received by the hydrophone located 1.2 mm above the membrane. (D) Peak-to-peak acoustic pressure profile within the donor, taken along the vertical direction (at a fixed *x-y* position centred with the membrane).

was ~ 19.5 mm, which is consistent with the separation distance with the bottom surface of the receptor. The acoustic pressure profile in the vertical direction (at a fixed x-y position, corresponding to the centre of the membrane) is reported in Fig. 4D, and provides a quantitative illustration of the acoustic pressure changes caused by the onset of an ultrasonic standing wave field. As discussed earlier, alternating acoustic pressure maxima and minima can be observed along the vertical direction. The average difference between these pressure maxima and minima is however equal to only 0.0306 MPa (corresponding to 2.5 % of the maximum peak-to-peak acoustic pressure), and it decreased as the distance from the artificial skin membrane increased. These pressure gradients are characteristic of a standing wave field and can result in the generation of different types of acoustic radiation forces. These forces can induce a translational motion of the microbubbles towards a pressure node (primary radiation forces), as well as aggregation of microbubbles (secondary, or Bjerknes, radiation forces) (Eller, 1968). Both these effects could be detrimental to the treatment efficacy and uniformity, as they may drive microbubbles away from a target surface and therefore limit the target surface area exposed to microbubble cavitation. However, given that acoustic pressure gradients in the developed Franz cell configuration are relatively weak and considering the pulsed nature of the US field applied, it is anticipated that these effects would be marginal. Moreover, the incident acoustic field will generate an additional radiation force of greater magnitude driving the MBs towards the skin model, that is likely to counteract the Bjerknes force and thus hinder potential microbubble aggregation (Janiak et al., 2023). Overall, these findings confirm that the developed ultrasound-integrated Franz cell apparatus can generate a highly predictable US field at the surface of a skin model, without any significant lateral distortion. A standing wave field is generated in the vertical direction, but this is sufficiently weak to expect only negligible effects on microbubbles suspended within the donor compartment. To the best of our knowledge, this is the first study reporting on a comprehensive quantitative characterisation of the ultrasound field generated within a Franz cell system by an integrated ultrasound transducer.

3.3. Identification of suitable ultrasound exposure parameters for microbubbles within the 3D-printed Franz cell donor

It is important to characterise the microbubble response and the liquid temperature increase in the donor induced by ultrasound exposure, as both factors are implicated in ultrasound-based treatment efficacy and safety. Both these effects are dependent on several factors, including the ultrasound frequency, pressure, and duration of exposure (Cool et al., 2013). The latter parameter was specifically evaluated in the present study. IMQ-loaded microbubbles were exposed to pulsed ultrasound at a frequency of 1.1 MHz, maximum peak-to-peak acoustic pressure of 1.2 MPa at the membrane, duty cycle of 50 %, and PRF of 200 Hz. Microbubble response was indirectly assessed from the reduction of MB concentration following US treatment, which is likely due to microbubble collapse and/or fragmentation (Klibanov et al., 2002). A significant reduction in MB concentration was observed for all US exposure times evaluated, as shown by the comparison between the microscopy images in Fig. 5A (pre-exposure to US) and 5B (post-exposure

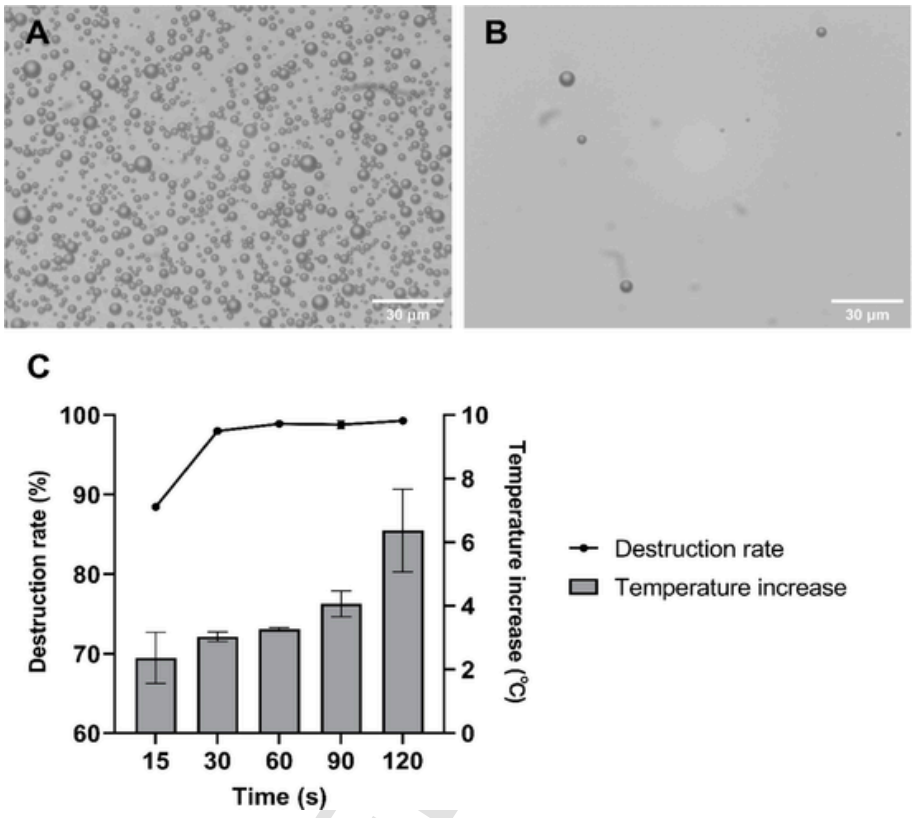

Fig. 5. Microscopy images (40x magnification) of air-filled microbubbles with a phospholipid shell consisting of DSPC:PEG40S (9:1 M ratio), (A) before and (B) after ultrasound exposure (ultrasound parameters: 1.1 MHz frequency, 1.2 MPa acoustic pressure at the membrane, 200 Hz PRF, and 50 % duty cycle). (C) The effect of US exposure time (in the range of 15–120 s) on microbubble destruction rate (shown by black dots and lines) and the liquid temperature increases in proximity to the StratM® membrane (shown by the grey bars). The applied US field had a frequency of 1.1 MHz, 50 % duty cycle, and acoustic peak-to-peak pressure of 1.2 MPa at the membrane (n = 3 independent experiments, mean ± SD).

to US). This observation is supported by previous studies that reported on the occurrence of inertial cavitation, collapse and/or fragmentation of microbubbles exposed to similar US parameters (Su et al., 2022). The percentage reduction in microbubble concentration, referred to as destruction rate, is reported in Fig. 5C for different ultrasound exposure times of 15, 30, 60, 90 and 120 s. The corresponding liquid temperature increase is also reported. The MB destruction rate increased from 88.45 ± 0.32 % at 15 s exposure to 97.98 ± 0.15 % at 30 s exposure, but then remained substantially unchanged with increasing the exposure time further. The greatest destruction rate was measured upon exposure to 120 s of ultrasound treatment and was equal to 99.28 ± 0.10 %. As shown in Fig. 5C, increasing the ultrasound exposure time resulted in increased liquid temperature in proximity to the skin model (StratM® membrane), ranging from 2.37 ± 0.66 °C (15 s exposure) to 6.37 ± 1.07 °C (120 s exposure). A 60 s ultrasound treatment induced a liquid temperature increase of 3.26 °C, which was higher than the temperature change reported in a previous study (1.1 °C) using a PDMS membrane exposed to similar conditions (1.1 MHz ultrasound, 60 s exposure time, and acoustic pressure of 100 kPa) (Yu et al., 2023). This difference can be likely attributed to the lower acoustic pressure employed in this previous study. It is important to note that increasing the ultrasound exposure time beyond 30 s caused a further increase in liquid temperature but did not improve the MB destruction rate further (ANOVA, $p > 0.05$). Therefore, this value was selected for subsequent drug permeation experiments, as a compromise between sufficient MB response and an acceptable temperature increase.

3.4. Applicability of the developed Franz cell system in the investigation of ultrasound- and microbubble-mediated sonophoresis

The developed Franz cell assembly underwent a proof-of-concept evaluation of feasibility for use for *in-vitro* drug permeation studies involving ultrasound-responsive drug delivery systems. IMQ-loaded gas microbubbles were employed as a model ultrasound-responsive agent in these tests; the corresponding drug encapsulation efficiency was 75 % (data not shown), resulting in the addition of 0.45 mg of drug to the donor compartment. In the first set of experiments, the performance of a cell comprising a 3D-printed donor (resin) was compared to that comprising a conventional glass donor, in the absence of ultrasound. The time evolution of the amount of IMQ that permeated into the receptor (Fig. 6A) and the amount of IMQ that penetrated into the membrane after 24 h (Fig. 6B) were quantified. Results show that there was no statistical difference between donor types, as indicated by the nearly overlapping temporal profiles in Fig. 6A and the comparable IMQ amount present in the membrane at 24 h (Fig. 6B). In particular, at the end of the experiment (24 h), IMQ permeation from the resin donor to the receptor was of 1.74 ± 0.29 µg and imiquimod partition into the membrane was of 2.29 ± 0.32 µg. Subsequently, experiments were conducted using the 3D-printed donor to assess potential permeation enhancement induced by ultrasound activated IMQ-loaded microbubbles. When microbubbles were employed (exposed to US for 30 s at frequency of 1.1 MHz and peak-to-peak acoustic pressure of 1.2 MPa), a more rapid drug permeation kinetics was observed. Moreover, at 3 h, the permeated imiquimod in the presence of ultrasound was quantified as 75.91 ± 14.50 µg, which represented the earliest detectable value in the receptor (above the limit of detection for the HPLC method). Conse-

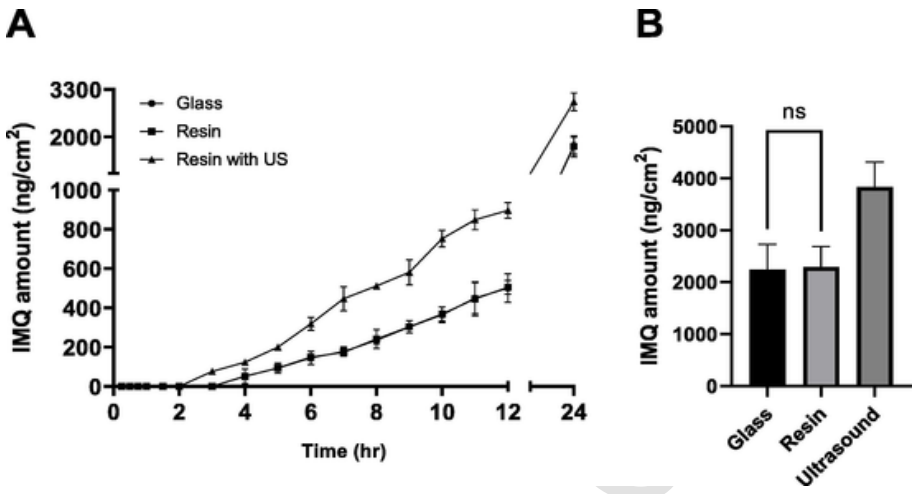

Fig. 6. *In-vitro* permeation studies of IMQ-loaded microbubbles. The experimental groups evaluated include the Franz cell with a glass donor in the absence of US (circles), and the Franz cell with a 3D-printed donor in the absence of US (squares) and in the presence of US (triangles). (A) The permeated amount of IMQ at different time points, up to 24 h, normalised to 1 cm^2 of the StratM® membrane. (B) The amount of IMQ that penetrated into the membrane after 24 h, normalized to 1 cm^2 of membrane surface (n = 3 independent experiments, mean ± SD, 'ns' means no statistical significance or $p > 0.05$).

quently, the onset of measurable drug permeation in the receptor took place earlier than in the absence of ultrasound (as shown in Fig. 6A). Perturbation of the skin model induced by microbubble cavitation was evident from the measured increase in both drug permeation (2.96 ± 0.25 μg, see Fig. 6A) and drug partition within the membrane (3.84 ± 0.39 μg, see Fig. 6B) after 24 h. These results indicate that the developed ultrasound-integrated Franz cell potentially provides a useful research tool for developing novel ultrasound-mediated permeation enhancement approaches that involve the use of ultrasound-responsive particulate systems, such as gas microbubbles or other nanoparticulate agents.

4. Conclusion

Transdermal drug delivery mediated by ultrasound has shown great potential in enhancing permeation of drugs across the skin. However, conventional Franz diffusion cells that are utilised in this research area often lack compatibility with ultrasound and ultrasound-responsive agents, because of material and design limitations or the lack of characterisation of the corresponding ultrasound field. To address these limitations, a new Franz cell donor compartment was designed and fabricated using 3D printing, and was then coupled with a conventional glass receptor to generate an ultrasound-integrated Franz cell assembly. The system was characterised for its physical performance and feasibility for use in drug permeation studies involving US-responsive microbubbles. The assembly was capable of effectively retaining liquids during prolonged incubation and a predictable ultrasound field could be generated at a target surface without any significant spatial distortion. Moreover, we have demonstrated the use of the novel Franz cell for evaluating sonophoresis of drug-loaded microbubbles. The device offers additional advantages compared to similar systems, including precise and repeatable positioning of the US source and high manufacture accuracy (< 0.5 mm) (Nulty, 2022). Moreover, the material used for 3D printing of the donor is cost-effective; the cost of manufacturing one resin donor is of approximately USD$5 (at the point of writing) and can be completed in just three hours, making it highly suitable for laboratory-scale iteration. The device is capable of meeting a wide range of sample requirements in sonophoresis, because of the availability of numerous materials that can be 3D printed via SLA, such as pH-resistant (Schmohl et al., 2022) and heat-resistant resins (Zhang et al., 2024). A drawback of the device lies in the occurrence of ultrasound reflection at the inner surfaces of the glass receptor compartment. The incorporation of an ultrasound absorbing material layer at the base of the receptor could be considered as an alternative approach to prevent acoustic reflections; however, it is necessary to assess its potential for undesired drug absorption. Alternative materials could also be evaluated for development of a 3D-printed receptor. These materials should have superior acoustic performance than glass as well as lower porosity than other resins, to prevent drug absorption onto the receptor's surface. This is particularly critical for the receptor compartment, as only trace amounts of drug may permeate through the skin.

CRediT authorship contribution statement

Xin Chen: Writing – review & editing, Writing – original draft, Visualization, Validation, Methodology, Investigation, Formal analysis, Data curation, Conceptualization. **Davide De Grandi:** Methodology, Investigation, Data curation. **Yonglian Zhu:** Methodology, Investigation, Data curation. **Gareth Lutheryn:** Methodology, Investigation, Data curation. **Majella Lane:** Writing – review & editing, Writing – original draft, Visualization, Supervision, Methodology, Investigation, Conceptualization. **Bruno Da Silva Sil Dos Santos:** Writing – review & editing, Writing – original draft, Visualization, Supervision, Methodology, Investigation, Conceptualization. **Dario Carugo:** Writing – review & editing, Writing – original draft, Visualization, Supervision, Project administration, Methodology, Investigation, Conceptualization.

Declaration of competing interest

The authors declare that they have no known competing financial interests or personal relationships that could have appeared to influence the work reported in this paper.

Acknowledgements

The authors would like to express their gratitude to Aaron Crowther (University College London), Liangyuan Xu (University College London) and Colm O'Reilly (University of Oxford) for their help with microbubble preparation.

Data availability

Data will be made available on request.

References

Ahmadi, F., McLoughlin, I.V., Chauhan, S., ter-Haar, G., 2012. Bio-effects and safety of low-intensity, low-frequency ultrasonic exposure. Prog. Biophys. Mol. Biol. 108, 119–138. https://doi.org/10.1016/j.pbiomolbio.2012.01.004.

Beamish, S., Reddyhoff, T., Hunter, A., Dwyer-Joyce, R.S., 2022. A method to determine acoustic properties of solids and its application to measuring oil film thickness in bearing shells of unknown composition. Measurement 195, 111176. https://doi.org/10.1016/j.measurement.2022.111176.

Bendicho-Lavilla, C., Díaz-Tomé, V., Seoane-Viaño, I., Luzardo-Álvarez, A.M., Otero-Espinar, F.J., 2024. Development of inert coatings to prevent drug retention in 3D-printed diffusion cells. Int. J. Pharm. 659, 124256. https://doi.org/10.1016/j.ijpharm.2024.124256.

Carugo, D., Aron, M., Sezgin, E., Bernardino de la Serna, J., Kuimova, M.K., Eggeling, C., Stride, E., 2017. Modulation of the molecular arrangement in artificial and biological membranes by phospholipid-shelled microbubbles. Biomaterials 113, 105–117. https://doi.org/10.1016/j.biomaterials.2016.10.034.

Cool, S.K., Geers, B., Roels, S., Stremersch, S., Vanderperren, K., Saunders, J.H., De Smedt, S.C., Demeester, J., Sanders, N.N., 2013. Coupling of drug containing liposomes to microbubbles improves ultrasound triggered drug delivery in mice. Journal of Controlled Release 172, 885–893. https://doi.org/10.1016/j.jconrel.2013.09.014.

Dahlan, A., Alpar, H.O., Murdan, S., 2009. An investigation into the combination of low frequency ultrasound and liposomes on skin permeability. Int. J. Pharm. 379, 139–142. https://doi.org/10.1016/j.ijpharm.2009.06.011.

Eller, A., 1968. Force on a Bubble in a Standing Acoustic Wave. J. Acoust. Soc. Am. 43, 170–171. https://doi.org/10.1121/1.1910755.

Formlabs, 2016. Clear Photoreactive Resin for Formlabs 3D printers Safety data sheet.

Gaertner, W., 1954. Frequency Dependence of Ultrasonic Cavitation. J. Acoust. Soc. Am. 26, 977–980. https://doi.org/10.1121/1.1907464.

Hakozaki, T., Takiwaki, H., Miyamoto, K., Sato, Y., Arase, S., 2006. Ultrasound enhanced skin-lightening effect of vitamin C and niacinamide. Skin Res. Technol. 12, 105–113. https://doi.org/10.1111/j.0909-752X.2006.00186.x.

Herwadkar, A., Sachdeva, V., Taylor, L.F., Silver, H., Banga, A.K., 2012. Low frequency sonophoresis mediated transdermal and intradermal delivery of ketoprofen. Int. J. Pharm. 423, 289–296. https://doi.org/10.1016/j.ijpharm.2011.11.041.

Isselin, J.-C., Alloncle, A.-P., Autric, M., 1998. On laser induced single bubble near a solid boundary: Contribution to the understanding of erosion phenomena. J. Appl. Phys. 84, 5766–5771. https://doi.org/10.1063/1.368841.

Janiak, J., Li, Y., Ferry, Y., Doinikov, A.A., Ahmed, D., 2023. Acoustic microbubble propulsion, train-like assembly and cargo transport. Nat. Commun. 14, 4705. https://doi.org/10.1038/s41467-023-40387-7.

Jung, E.C., Zhu, H., Zou, Y., Elmahdy, A., Cao, Y., Hui, X., Maibach, H.I., 2016. Effect of ultrasound and heat on percutaneous absorption of ascorbic acid: humanin vitro studies on Franz cell and Petri dish systems. Int. J. Cosmet. Sci. 38, 646–650. https://doi.org/10.1111/ics.12350.

Klibanov, A.L., Hughes, M.S., Wojdyla, J.K., Wible, J.H., Brandenburger, G.H., 2002. Destruction of Contrast Agent Microbubbles in the Ultrasound Field. Acad. Radiol. 9, S41–S45. https://doi.org/10.1016/S1076-6332(03)80393-8.

Kotopoulis, S., Lam, C., Haugse, R., Snipstad, S., Murvold, E., Jouleh, T., Berg, S., Hansen, R., Popa, M., Mc Cormack, E., Gilja, O.H., Poortinga, A., 2022. Formulation and characterisation of drug-loaded antibubbles for image-guided and ultrasound-triggered drug delivery. Ultrason. Sonochem. 85, 105986. https://doi.org/10.1016/j.ultsonch.2022.105986.

Lentacker, I., De Smedt, S.C., Sanders, N.N., 2009. Drug loaded microbubble design for ultrasound triggered delivery. Soft Matter 5, 2161. https://doi.org/10.1039/b823051j.

Liao, A.-H., Shih, C.-P., Li, M.-W., Lin, Y.-C., Chuang, H.-C., Wang, C.-H., 2021. Development of thermosensitive poloxamer 407-based microbubble gel with ultrasound mediation for inner ear drug delivery. Drug Deliv. 28, 1256–1271. https://doi.org/10.1080/10717544.2021.1938758.

Liu, S., Zhang, Y., Liu, Y., Wang, W., Gao, S., Yuan, W., Sun, Z., Liu, L., Wang, C., 2023. Ultrasound-targeted microbubble destruction remodels tumour microenvironment to improve immunotherapeutic effect. Br. J. Cancer 128, 715–725. https://doi.org/10.1038/s41416-022-02076-y.

Meidan, V.M., Walmsley, A.D., Docker, M.F., Irwin, W.J., 1999. Ultrasound-enhanced diffusion into coupling gel during phonophoresis of 5-fluorouracil. Int. J. Pharm. 185, 205–213. https://doi.org/10.1016/S0378-5173(99)00168-4.

Mitragotri, S., Kost, J., 2001. Transdermal delivery of heparin and low-molecular weight heparin using low-frequency ultrasound. Pharm. Res. 18, 1151–1156. https://doi.org/10.1023/A:1010979010907.

Mohmmed, S.A., Vianna, M.E., Hilton, S.T., Boniface, D.R., Ng, Y.-L., Knowles, J.C., 2017. Investigation to test potential stereolithography materials for development of an in vitro root canal model. Microsc. Res. Tech. 80, 202–210. https://doi.org/10.1002/jemt.22788.

Norman, J., Madurawe, R.D., Moore, C.M.V., Khan, M.A., Khairuzzaman, A., 2017. A new chapter in pharmaceutical manufacturing: 3D-printed drug products. Adv. Drug Deliv. Rev. 108, 39–50. https://doi.org/10.1016/j.addr.2016.03.001.

Nulty, A., 2022. A comparison of trueness and precision of 12 3D printers used in dentistry. BDJ Open 8, 14. https://doi.org/10.1038/s41405-022-00108-6.

Palanisamy, A., Salim, N.V., Parameswaranpillai, J., Hameed, N., 2017. Water Sorption and Solvent Sorption of Epoxy/Block-Copolymer and Epoxy/Thermoplastic Blends. In: Handbook of Epoxy Blends. Springer International Publishing, Cham, pp. 1097–1111. https://doi.org/10.1007/978-3-319-40043-3_40.

Park, D., Ryu, H., Kim, H.S., Kim, Y., Choi, K.-S., Park, H., Seo, J., 2012. Sonophoresis using ultrasound contrast agents for transdermal drug delivery: an in vivo experimental study. Ultrasound Med. Biol. 38, 642–650. https://doi.org/10.1016/j.ultrasmedbio.2011.12.015.

Park, E.J., Werner, J., Smith, N.B., 2007. Ultrasound mediated transdermal insulin delivery in pigs using a lightweight transducer. Pharm. Res. 24, 1396–1401. https://doi.org/10.1007/s11095-007-9306-4.

Park, D., Won, J., Shin, U., Park, H., Song, G., Jang, J., Park, H., Kim, C.-W., Seo, J.B., 2019. Transdermal drug delivery using a specialized cavitation seed for ultrasound. IEEE Trans. Ultrason. Ferroelectr. Freq. Control 66, 1057–1064. https://doi.org/10.1109/TUFFC.2019.2907702.

Park, D., Won, J., Lee, G., Lee, Y., Kim, C., Seo, J., 2022. Sonophoresis with ultrasound-responsive liquid-core nuclei for transdermal drug delivery. Skin Res. Technol. 28, 291–298. https://doi.org/10.1111/srt.13129.

Paula, D.D., Martins, C.A., Bentley, M.V.L.B., 2008. Development and validation of HPLC method for imiquimod determination in skin penetration studies. Biomed. Chromatogr. 22, 1416–1423. https://doi.org/10.1002/bmc.1075.

Pero, A.C., Marra, J., Paleari, A.G., de Souza, R.F., Ruvolo-Filho, A., Compagnoni, M.A., 2011. Reliability of a method for evaluating porosity in denture base resins. Gerodontology 28, 127–133. https://doi.org/10.1111/j.1741-2358.2009.00347.x.

Petrilli, R., Lopez, R.F.V., 2018. Physical methods for topical skin drug delivery: concepts and applications. Braz. J. Pharm. Sci. 54.

Polat, B.E., Hart, D., Langer, R., Blankschtein, D., 2011. Ultrasound-mediated transdermal drug delivery: Mechanisms, scope, and emerging trends. J. Control. Release 152, 330–348. https://doi.org/10.1016/j.jconrel.2011.01.006.

Robertson, J., Becker, S., 2015. Motivations for a custom apparatus for sonophoresis experimentation. IFAC-PapersOnLine 48, 100–105. https://doi.org/10.1016/j.ifacol.2015.10.122.

Robertson, J., Becker, S., 2018. Influence of acoustic reflection on the inertial cavitation dose in a franz diffusion cell. Ultrasound Med. Biol. 44, 1100–1109. https://doi.org/10.1016/j.ultrasmedbio.2018.01.021.

Saito, S., 2015. Ultrasound Field and Bubbles, in: Sonochemistry and the Acoustic Bubble. Elsevier, pp. 11–39. doi: 10.1016/B978-0-12-801530-8.00002-5.

Salonitis, K., 2014. Stereolithography, in: Comprehensive Materials Processing. Elsevier, pp. 19–67. doi: 10.1016/B978-0-08-096532-1.01001-3.

Schmohl, L., Roesner, A.J., Fuchs, F., Wagner, M., Schmidt, M.B., Hahnel, S., Rauch, A., Koenig, A., 2022. Acid Resistance of CAD/CAM Resin Composites. Biomedicines 10, 1383. https://doi.org/10.3390/biomedicines10061383.

Schoellhammer, C.M., Polat, B.E., Mendenhall, J., Maa, R., Jones, B., Hart, D.P., Langer, R., Blankschtein, D., 2012. Rapid skin permeabilization by the simultaneous application of dual-frequency, high-intensity ultrasound. J. Control. Release 163, 154–160. https://doi.org/10.1016/j.jconrel.2012.08.019.

Sen, T., Tufekcioglu, O., Koza, Y., 2015. Mechanical index. Anadolu Kardiyoloji Dergisi/the Anatolian Journal of Cardiology 15, 334–336. https://doi.org/10.5152/akd.2015.6061.

Sil, B.C., Alvarez, M.P., Zhang, Y., Kung, C.-P., Hossain, M., Iliopoulos, F., Luo, L., Crowther, J.M., Moore, D.J., Hadgraft, J., Lane, M.E., Hilton, S.T., 2018. 3D-printed Franz type diffusion cells. Int. J. Cosmet. Sci. 40, 604–609. https://doi.org/10.1111/ics.12504.

Sil, B.C., Belgrave, R.G., Alvarez, M.P., Luo, L., Cristofoli, M., Penny, M.R., Moore, D.J., Hadgraft, J., Hilton, S.T., Lane, M.E., 2020. 3D-Printed Franz cells – update on optimization of manufacture and evaluation. Int. J. Cosmet. Sci. 42, 415–419. https://doi.org/10.1111/ics.12618.

Simon, A., Amaro, M.I., Healy, A.M., Cabral, L.M., de Sousa, V.P., 2016. Comparative evaluation of rivastigmine permeation from a transdermal system in the Franz cell using synthetic membranes and pig ear skin with in vivo-in vitro correlation. Int. J. Pharm. 512, 234–241. https://doi.org/10.1016/j.ijpharm.2016.08.052.

Sindhu, P.S., Mitra, N., Ghindani, D., Prabhu, S.S., 2021. Epoxy Resin (DGEBA/TETA) exposed to water: a spectroscopic investigation to determine water-epoxy interactions. J. Infrared Millim Terahertz Waves 42, 558–571. https://doi.org/10.1007/s10762-021-00788-5.

Skelly, J.P., Shah, V.P., Maibach, H.I., Guy, R.H., Wester, R.C., Flynn, G., Yacobi, A., 1987. FDA and AAPS report of the workshop on principles and practices of in vitro percutaneous penetration studies: relevance to bioavailability and bioequivalence. Pharm. Res. 4, 265–267. https://doi.org/10.1023/A:1016428716506.

Souza, J., Meira, A., Volpato, N.M., Mayorga, P., Gottfried, C., 2013. Effect of Phonophoresis on Skin Permeation of Commercial Anti-inflammatory Gels: Sodium Diclofenac and Ketoprofen. Ultrasound Med. Biol. 39, 1623–1630. https://doi.org/10.1016/j.ultrasmedbio.2013.02.009.

Stirling, J.W., Woods, A.E., 2019. Resin (plastic) embedding for microscopy and tissue analysis, in: Bancroft's Theory and Practice of Histological Techniques. Elsevier, pp. 96–113. doi: 10.1016/B978-0-7020-6864-5.00008-6.

Su, C., Ren, X., Yang, F., Li, B., Wu, H., Li, H., Nie, F., 2022. Ultrasound-sensitive siRNA-loaded nanobubbles fabrication and antagonism in drug resistance for NSCLC. Drug Deliv. 29, 99–110. https://doi.org/10.1080/10717544.2021.2021321.

Subongkot, T., 2020. Combined effect of sonophoresis and a microemulsion on the dermal delivery of celecoxib. Drug Deliv. 27, 1087–1093. https://doi.org/10.1080/10717544.2020.1797244.

D Systems, 2014. Accura® ClearVue™ Safety Data Sheet.

Tiboni, M., Curzi, G., Aluigi, A., Casettari, L., 2021. An easy 3D printing approach to manufacture vertical diffusion cells for in vitro release and permeation studies. J. Drug Deliv. Sci. Technol. 65, 102661. https://doi.org/10.1016/j.jddst.2021.102661.

Trogé, A., O'Leary, R.L., Hayward, G., Pethrick, R.A., Mullholland, A.J., 2010. Properties

of photocured epoxy resin materials for application in piezoelectric ultrasonic transducer matching layers. J. Acoust. Soc. Am. 128, 2704–2714. https://doi.org/10.1121/1.3483734.

Tyle, P., Agrawala, P., 1989. Drug delivery by phonophoresis. Pharm. Res. 6, 355–361. https://doi.org/10.1023/A:1015967012253.

Wang, H.-L., Fan, P.-F., Guo, X.-S., Tu, J., Ma, Y., Zhang, D., 2016. Ultrasound-mediated transdermal drug delivery of fluorescent nanoparticles and hyaluronic acid into porcine skin *in vitro*. Chin. Phys. B 25, 124314. https://doi.org/10.1088/1674-1056/25/12/124314.

Wolloch, L., Kost, J., 2010. The importance of microjet vs shock wave formation in sonophoresis. J. Control. Release 148, 204–211. https://doi.org/10.1016/j.jconrel.2010.07.106.

Yamashita, N., Tachibana, K., Ogawa, K., Tsujita, N., Tomita, A., 1997. Scanning electron microscopic evaluation of the skin surface after ultrasound exposure. Anat. Rec. 247, 455–461. https://doi.org/10.1002/(SICI)1097-0185(199704)247:4<455::AID-AR3>3.0.CO;2-Q.

Yu, C., Shah, A., Amiri, N., Marcus, C., Nayeem, M.O.G., Bhayadia, A.K., Karami, A., Dagdeviren, C., 2023. A conformable ultrasound patch for cavitation-enhanced transdermal cosmeceutical delivery. Adv. Mater. 35. https://doi.org/10.1002/adma.202300066.

Zaleski, R., Stefaniak, W., Maciejewska, M., Goworek, J., 2009. Porosity of polymer materials by various techniques. J. Porous Mater. 16, 691–698. https://doi.org/10.1007/s10934-008-9250-7.

Zhang, C., Liu, Z., Wang, X., Zhang, Q., Xing, W., Zhang, T., Chi, Q., 2024. Research on molecular dynamics and electrical properties of high heat-resistant epoxy resins. J. Chem. Phys. 160. https://doi.org/10.1063/5.0197089.

Zhang, N., Wu, Y., Xing, R., Xu, B., Guoliang, D., Wang, P., 2017. Effect of ultrasound-enhanced transdermal drug delivery efficiency of nanoparticles and brucine. Biomed Res. Int. 2017, 1–8. https://doi.org/10.1155/2017/3273816.